Peierls transitions in quasi-one-dimensional conductor Nb_3Te_4 and the effect of metal–atom intercalation, investigated by ^{93}Nb magnetic resonance

2002 J. Phys.: Condens. Matter 14 7503

(http://iopscience.iop.org/0953-8984/14/32/310)

INSTITUTE OF PHYSICS PUBLISHING JOURNAL OF PHYSICS: CONDENSED MATTER

J. Phys.: Condens. Matter **14** (2002) 7503–7512 PII: S0953-8984(02)33185-0

Peierls transitions in quasi-one-dimensional conductor Nb_3Te_4 and the effect of metal–atom intercalation, investigated by ^{93}Nb magnetic resonance

H Ishida[1], T Koyama[1], T Mito[2], S Wada[1,2] and Y Ishihara[3]

[1] Department of Material Science, Graduate School of Science and Technology, Kobe University, Nada, Kobe 657-8501, Japan
[2] Department of Physics, Faculty of Science, Kobe University, Nada, Kobe 657-8501, Japan
[3] Department of Physics, Faculty of Science, Kanazawa University, Kanazawa 920-1192, Japan

Received 30 January 2002, in final form 21 June 2002
Published 2 August 2002
Online at stacks.iop.org/JPhysCM/14/7503

Abstract

We have carried out a ^{93}Nb nuclear magnetic resonance (NMR) study on a quasi-one-dimensional superconductor, Nb_3Te_4, and the isostructural intercalated compounds $A_xNb_3Te_4$ (A = In and Zn), to understand the varied impact of metal–atom intercalations into the hexagonal infinite tunnels on the charge density wave and superconductivity formations. Below the Peierls transition temperature T_C for each of the compounds, the nuclear spin–lattice relaxation rate $(T_1T)^{-1}$ exhibited a significant decrease which originates from the partial Fermi surface quenching associated with the Peierls transition. With $x \simeq 0.1$ introductions of In and Zn, $(T_1T)^{-1}$ was greatly enhanced from 10 $s^{-1}K^{-1}$ to 20 and 18 $s^{-1}K^{-1}$, respectively. On the other hand, the nuclear quadrupole frequency ν_Q was diminished from 0.98 MHz to 0.63 and 0.74 MHz, respectively. A remarkable difference between the In and Zn intercalations was found in the extent of decrease in the isotropic Knight shift K_{iso}: from 0.237 to 0.216% for In; and to 0.166% for Zn. Based upon the d band structures predicted theoretically, we have indicated that the variations in the NMR parameters can be explained consistently, if the extent of hole doping by a Zn atom is much larger than that by an In atom. The heavy hole doping by Zn intercalation changes the dominant subband at E_F from $d_{yz,zx}$ to $d_{x^2-y^2}$, giving rise to a distinct nesting condition of the Fermi surface.

1. Introduction

The triniobium tetrachalcogenide series Nb_3X_4 (X = S, Se and Te) with isomorphous crystal structure ($P6_3/m$) [1–3] has attracted considerable interest because of the unusual electrical transport properties, anisotropic superconductivity and metal–atom intercalation. The crystal has zigzag Nb chains along the c axis, and the intrachain Nb–Nb distance is nearly equal to

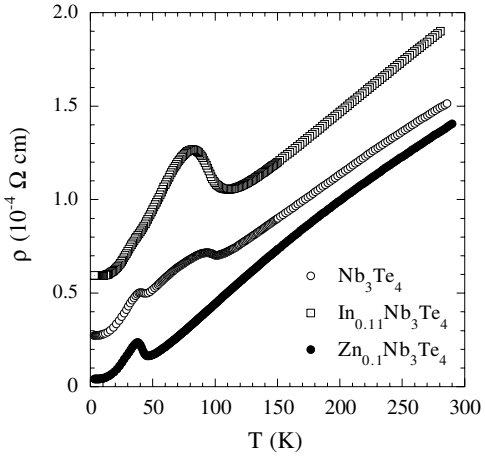

Figure 1. Temperature dependence of electrical resistivity for each of Nb_3Te_4, $In_{0.11}Nb_3Te_4$ and $Zn_{0.1}Nb_3Te_4$.

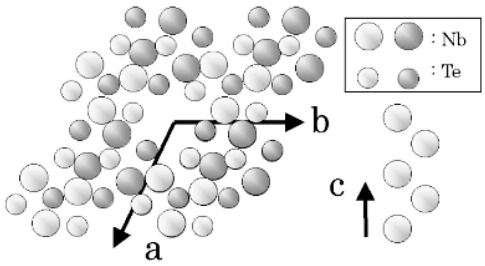

Figure 2. Crystal structure of Nb_3Te_4. (a) View down the $c(z)$ axis. Atoms on the plane with $z = c/4$ are drawn by dark circles and those with $z = 3c/4$ are drawn by bright circles. (b) Zigzag Nb chain along the c direction.

that of niobium metal. However, the interchain Nb–Nb distance is separated by surrounding chalcogen atoms and, therefore, the one-dimensional properties are expected to be more marked on increasing the radius of chalcogen atom from S to Te atoms. Nb_3S_4 (superconducting transition temperature $T_S = 3.78$ K [4]) and Nb_3Se_4 ($T_S = 2.31$ K [4]) are strongly anisotropic metals, and the electrical resistivity along the c axis exhibits a T^3 dependence below about 80 K [5, 6] which could be explained in terms of the quasi-one-dimensional band structure and electron–electron Umklapp scattering processes [7].

For Nb_3Te_4 ($T_S = 1.9$ K), there are anomalies at $T_{C1} \sim 110$ K and $T_{C2} \sim 45$ K (defined at threshold temperature) [8] in the electrical resistivity shown in figure 1 and in the thermoelectric power. It was concluded by electron [9] and x-ray diffraction [10] measurements that the T_{C1} anomaly is associated with a commensurate charge density wave (CDW) formation with wavevectors of $\boldsymbol{q} = \pm(a^*/3, b^*/3), +3c^*/7$. No superlattice was observed to be associated with the T_{C2} anomaly.

The hexagonal unit cell of Nb_3X_4 contains six Nb atoms and eight chalcogens as shown in figure 2(a). Each Nb atom is surrounded by six chalcogens at the corner of a deformed NbX_6 octahedron, and each octahedron is linked to two other octahedra by common faces and to four octahedra by common edges. The Nb atoms are shifted from the centre of the octahedron in the direction of faces sharing two edges with other octahedra. Hence the zigzag Nb chains are formed along the c axis as shown in figure 2(b).

It is notable that the three-dimensional network of NbX_6 octahedra forms infinite empty hexagonal tunnels along the c axis. A large number of metal atoms can be introduced into the tunnels to form a family of isostructural intercalated compounds, $A_xNb_3Te_4$ (A = Na, K, Tl, Cu, Ag, In, Ca, Zn, Pb, Bi, La etc) [11, 12]. The intercalated atoms have been considered to contribute holes to the conduction d bands, and affect significantly both the superconductivity and CDW formations [13]. With increasing extent of Hg intercalation, T_S shows an initial steep increase from 1.9 to 5.4 K for $x = 0$–0.4. Ohtani *et al* [14] reported for $In_xNb_3Te_4$ ($x = 0$–0.6) that the electrical resistivity anomaly at T_{C1} is more clearly observed with the increase of T_{C1} to $\sim$160 K, while the small anomaly at T_{C2} almost disappears. In contrast, for $Zn_xNb_3Te_4$ the anomaly at T_{C1} completely disappears and that at T_{C2} is enhanced. The temperature dependence of the electrical resistivity for each of $In_{0.11}Nb_3Te_4$ ($T_S = 2.6$ K) and $Zn_{0.1}Nb_3Te_4$ ($T_S = 2.1$ K) is shown in figure 1. For the light intercalation of $x \simeq 0.1$ into the hexagonal tunnels, the lattice constants are hardly affected [13, 14].

In this paper, we report the results of a nuclear magnetic resonance (NMR) measurement of ^{93}Nb in Nb_3Te_4, $In_{0.11}Nb_3X_4$ and $Zn_{0.1}Nb_3X_4$ to deduce the electronic states and the variation with the metal–atom intercalation, that can clearly define the physics of this system. The nuclear spin–lattice relaxation rate $(T_1T)^{-1}$ gives a measure of $N(E_F)$. The extent of hole doping by the intercalation is estimated through the variations in the nuclear quadrupole frequency ν_Q and the d orbital Knight shift K_{VV}.

2. Experimental details

Single crystals of Nb_3X_4 were prepared by an iodine-vapour-transport method following Nakada and Ishihara [15, 16] on the basis of the earlier work [2, 4]. $A_xNb_3X_4$ were obtained by means of exposing Nb_3X_4 to the ternary element vapour [13]. Grown crystals were always fibres and were crushed into powder with grain size smaller than the skin depth for the NMR measurement.

The NMR experiment was carried out utilizing a wide-band phase-coherent spin-echo spectrometer in temperature ranges between 4.2 and 200 K for Nb_3Te_4, 4.2 and 180 K for $In_{0.11}Nb_3Te_4$ and 4.2 and 100 K for $Zn_{0.1}Nb_3Te_4$. NMR spectra of ^{93}Nb (gyromagnetic ratio $\gamma_n = 1.0405$ kHz Oe^{-1}, nuclear spin $I = 9/2$, electric quadrupole moment $Q = -0.22$ barns) were obtained in a field sweeping procedure at a constant frequency of 75 MHz (figure 3).

In high magnetic fields, the expression for the frequency of transition between the nuclear spin states m and $m-1$ for nuclei located at the site with an axially symmetric electric field gradient (EFG) q is given by [17]

$$\nu(\theta) = \frac{\gamma_n}{2\pi}H[1 + K_{iso} + K_{ax}(3\cos^2\theta - 1)] + \frac{1}{2}\nu_Q\left(m - \frac{1}{2}\right)(3\cos^2\theta - 1) + \left(\frac{1}{32\nu_0}\right)\nu_Q^2 f_m(\theta), \tag{2.1}$$

where

$$\nu_Q = |3e^2qQ/2hI(2I-1)| \tag{2.2}$$

and

$$f_m(\theta) = \sin^2\theta([102m(m-1) - 18I(I+1) + 39]\cos^2\theta - [6m(m-1) - 2I(I+1) + 3]). \tag{2.3}$$

K_{iso} and K_{ax} are the isotropic and axial Knight shifts, and θ is the angle between the applied magnetic field H and the symmetry axis of the EFG. For powdered specimens, intensity

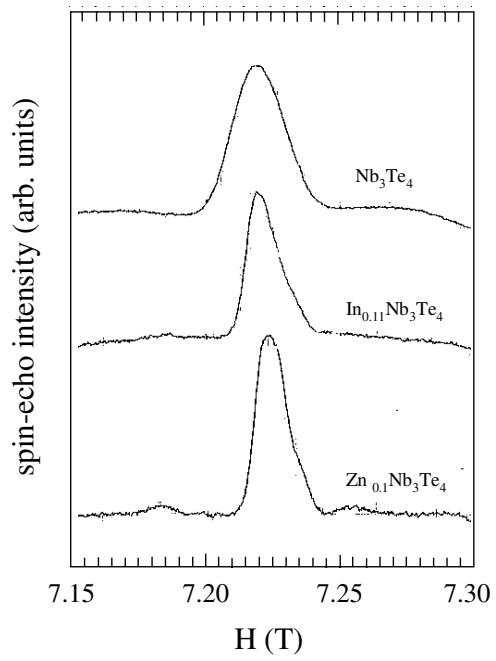

Figure 3. ^{93}Nb NMR spectra for each of Nb_3Te_4, $In_{0.11}Nb_3Te_4$ and $Zn_{0.1}Nb_3Te_4$ observed at 75 MHz and 80 K.

maxima occur at $\theta = \pi/2$, giving rise to $(I - 1/2)$ satellite pairs at the frequency of $\nu(\theta) = (\gamma_n/2\pi)H[1+K_{\rm iso}-K_{\rm ax}]-(1/2)\nu_{\rm Q}(m-1/2)-(1/32\nu_0)\nu_{\rm Q}^2[6m(m-1)-2I(I+1)+3]$. The intensity maxima displayed in figure 3 can be assigned to a central line and a first satellite pair. From the interval between the first satellite pair, we obtained values of the quadrupole frequency $\nu_{\rm Q}$. Figure 4 shows the temperature dependence of $\nu_{\rm Q}$ for each of the compounds. For Nb_3Te_4 and $In_{0.11}Nb_3Te_4$, $\nu_{\rm Q}$ of ^{93}Nb exhibits a nearly temperature-independent behaviour at high temperatures followed by a monotonic increase below about 100 K. On the other hand, $\nu_{\rm Q}$ for $Zn_{0.1}Nb_3Te_4$ simply exhibits the nearly temperature-independent behaviour down to 4.2 K. The intercalations of 0.11 at.% In and 0.1 at.% Zn reduced the value of $\nu_{\rm Q}$ at high temperatures from $\simeq$0.98 MHz for Nb_3Te_4 to $\simeq$0.63 and 0.74 MHz, respectively.

The second-order electric quadrupole interaction splits the central line with maxima at $\theta = \pi/2$ and $\cos^{-1}\sqrt{5/9}$ [17]. In addition to the effect of second-order quadrupole interaction, the axial Knight shift may also give rise to a certain characteristic line shape. When the major axes of the EFG and Knight shift tensors are coincident, following Jones *et al* [18] and McCart [19], the central line splits with maxima at $\cos\theta_{\rm I} = 0$ and at

$$\cos\theta_{\rm II} = \pm\left\{\frac{5}{9} - \frac{8a\nu_0^2}{3\nu_Q^2[I(I+1)-3/4]}\right\}^{\frac{1}{2}} \tag{2.4}$$

where $a = K_{\rm ax}/[1 + K_{\rm iso}]$. The splitting of the central line is given by [18]

$$\Delta_{\rm I,II} = \frac{25b}{9\nu_0} - \frac{5a\nu_0}{3} + \frac{a^2{\nu_0}^3}{4b} : \tag{2.5}$$

the anisotropic effect of the Knight shift is proportional to H, whereas the second-order quadrupole splitting is proportional to $1/H$.

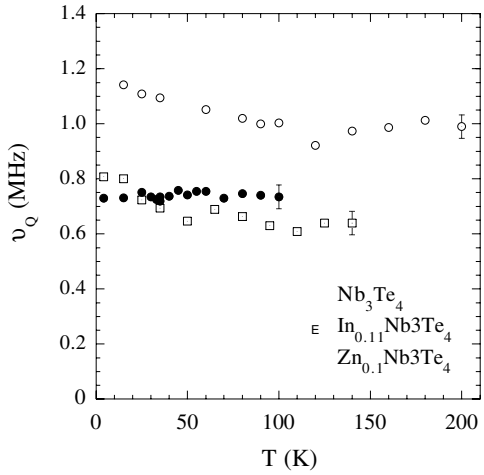

Figure 4. Dependence of ^{93}Nb quadrupole frequency ν_Q on the temperature for each of Nb_3Te_4, $In_{0.11}Nb_3Te_4$ and $Zn_{0.1}Nb_3Te_4$.

The central line of the ^{93}Nb resonance spectrum observed for each of the compounds, however, did not exhibit the splitting but was somewhat anisotropic in shape (figure 3). The full linewidth at half maximum observed at 75.0 and 37.5 MHz was proportional to $1/H$, which is indicative of a dominant second-order quadrupole broadening ($K_{ax} \simeq 0$). A small splitting of the central line, $\Delta_{I,II}/\gamma_n \sim 50$ Oe, calculated taking the experimental ν_Q value, is considered to be smeared out by the NMR perturbing field H_1 of $\simeq$100 Oe. Then we defined the isotropic Knight shift K_{iso} at the peak intensity of the central line, which brings a somewhat large experimental uncertainty of $\pm 0.015\%$. K_{iso} for each of the compounds was nearly independent of the temperature. $K_{iso} = 0.237\%$ for Nb_3Te_4 was reduced to 0.216% with the 0.11 at.% In intercalation, but greatly reduced to 0.166% with the 0.1 at.% Zn intercalation.

The nuclear spin–lattice relaxation time T_1 was measured at the peak intensity of the central resonance line, utilizing a radio-frequency (rf) comb-pulse saturation method. The experimental magnetization $M(t)$ at t after the saturation rf pulses showed a multiexponential recovery. Figure 5 shows $[M(\infty) - M(t)]$ data plotted against tT for Nb_3Te_4 obtained at 15, 60 and 160 K. As can be seen in the figure, the characteristic of the magnetization recovery does not vary with temperature. The theoretical recovery curve is given by [20]

$$\frac{M(\infty) - M(t)}{M(\infty)} = a_1 e^{-t/T_1} + a_2 e^{-6t/T_1} + a_3 e^{-15t/T_1} + a_4 e^{-28t/T_1} + a_5 e^{-45t/T_1}, \tag{2.6}$$

where a_i depends on the initial saturation condition imposed on all the nuclear spin levels. We could not, however, reproduce the experimental recovery data by equation (2.6) with reasonable values of a_i. Then, we assigned a characteristic time $T_1^{(e)}$ at which $[M(\infty) - M(t)]$ reaches $1/e$ of its initial value. Figure 6 shows the temperature dependence of $T_1^{(e)}$ for each of the compounds plotted on a log–log scale. $T_1^{(e)}$ follows a Korringa-like relation ($T_1^{(e)}T =$ constant) at high temperatures, and exhibits a significant increase below about 50 K for both Nb_3Te_4 and $In_{0.11}Nb_3Te_4$, and below about 30 K for $Zn_{0.1}Nb_3Te_4$. The values of K_{iso}, $T_1^{(e)}T$ and ν_Q are summarized in table 1.

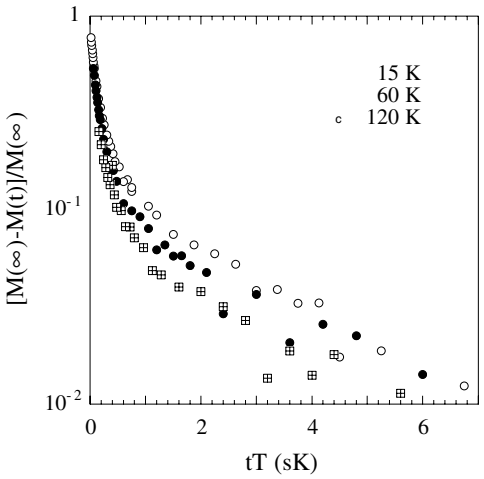

Figure 5. Experimental magnetization recovery behaviour of ^{93}Nb in Nb_3Te_4 observed typically at 15, 60 and 60 K.

Table 1. Knight shift K_{iso}, nuclear spin–lattice relaxation rate $T_1^{(e)}T$, and nuclear quadrupole frequency ν_Q of ^{93}Nb.

	K_{iso} (%)	$(T_1T)^{-1}$ $s^{-1}K^{-1}$		ν_Q (MHz)
		High T	Low T	
Nb_3Te_4	0.237	10	7.7	0.98
0.11 at.% In intercalation	0.216	20	6.3	0.63
0.1 at.% Zn intercalation	0.166	18	12.8	0.74

3. Discussion

Nb_3Te_4 consists of zigzag Nb chains which are linked via Te atoms. The electronic structure of Nb_3Te_4 has been calculated theoretically using the atomic-orbital method by Bullett [21], the linear combination of atomic orbitals method by Oshiyama [22, 23] and the tight-binding approximation by Canadell and Whangbo [24]. Reflecting the quasi-one-dimensional feature of the crystal structure, the energy band structure shows many narrow peaks which consist of mixed 4d orbitals of Nb, and the Fermi level E_F is located near a minimum of the d density of states (DOS) curve, giving rise to a small $N(E_F)$. The Fermi surface of Nb_3Te_4 consists of three warped or undulating planelike sheets associated with t_{2g} subbands mainly of d_{yz} and d_{zx} subbands. The $d_{x^2-y^2}$ subband is located somewhat lower in energy below the Fermi level [22–24]. Based on the theoretical calculations, $N(E_F)$ would be greatly changed in magnitude with the extent of metal–atom intercalations into the hexagonal tunnels.

We first discuss the electronic state of Nb_3Te_4 utilizing the data of Knight shift K_{iso}, relaxation rate $(T_1^{(e)}T)^{-1}$ and quadrupole frequency ν_Q. For the transition-metal elements, K and $(T_1T)^{-1}$ consist mainly of the d spin and Van Vleck orbital terms and, in the independent-electron tight-binding model, can be represented as [25]

$$K = K_d + K_{VV} = 2\mu_B H_{hf}^{d} N(E_F) + [H_{hf}^{orb}/\mu_B]\chi_{VV} \tag{3.1}$$

and

$$(T_1T)^{-1} = (T_1T)_d^{-1} + (T_1T)_{VV}^{-1} = 4\pi\gamma_n^2\hbar k_B[(H_{hf}^{d})^2 q_d + (H_{hf}^{orb})^2 p_d]N(E_F)^2, \tag{3.2}$$

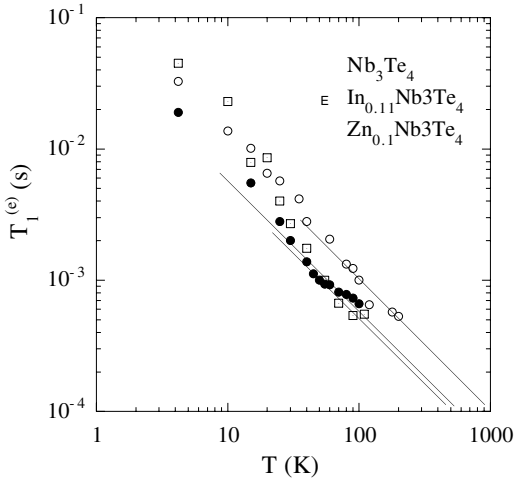

Figure 6. T_1 data plotted against temperature in a log–log plot for each of Nb_3Te_4, $In_{0.11}Nb_3Te_4$ and $Zn_{0.1}Nb_3Te_4$.

where $H_{\rm hf}^{\rm d}$ and $H_{\rm hf}^{\rm orb}$ are the d spin and orbital hyperfine fields, and $\chi_{\rm VV}$ is the field-induced orbital paramagnetic susceptibility that arises from the orbital degeneracy of the atomic d states. p_d and q_d are the reduction factors which depend on the relative weights at $E_{\rm F}$ of atomic d wavefunctions. The quadrupole frequency $\nu_{\rm Q}$ relates to the EFG q and the quadrupole moment Q of an observed nucleus as $\nu_{\rm Q} = |3e^2qQ/2hI(2I-1)|$. q consists of contributions $q_{\rm lat}$ from the ionic charge on the lattice sites around the observed nucleus, and $q_{\rm el}$ from the intra-atomic electron distribution as [26]

$$q = (1 - r_\infty)q_{\rm lat} + (1 + R)q_{\rm el}, \tag{3.3}$$

where

$$q_{\rm el} = \Sigma n_i \left\langle \frac{3z^2 - r^2}{r^5} \right\rangle_i . \tag{3.4}$$

n_i is the occupation number in the ith d orbital, and r_∞ and R are ionic Sternheimer antishielding factor and core correction factor, respectively.

The temperature-independent behaviour of both $K_{\rm iso}$ and $T_1^{(e)}T$ of Nb_3Te_4 at high temperatures is the characteristic of prototypical Pauli paramagnetism. Following the energy band structure calculated theoretically [21, 23], the d band around $E_{\rm F}$ consists mainly of d_{yz} and d_{zx} subbands. Nearly filled $d_{x^2-y^2}$ and empty $d_{3z^2-r^2,xy}$ subbands are located below and above $E_{\rm F}$, respectively. Then, following Obata [27], the reduction factors p_d and q_d in equation (3.2) are given by

$$p_d = C_{yz}^2 + C_{zx}^2 + C_{x^2-y^2}^2 \tag{3.5}$$

and

$$q_d = \tfrac{1}{2}[C_{yz}C_{x^2-y^2} + C_{zx}C_{x^2-y^2}], \tag{3.6}$$

where $C_{yz}/5$, $C_{zx}/5$ and $C_{x^2-y^2}/5$ are the degrees of admixture at $E_{\rm F}$ of the atomic wavefunctions d_{yz}, d_{zx} and $d_{x^2-y^2}$, respectively. For the dominant $d_{yz,zx}$ subbands at $E_{\rm F}$, C_{yz}, $C_{zx} \gg C_{x^2-y^2}$ and, therefore, $(T_1T)^{-1}$ is dominated by the d spin relaxation term $(T_1T)_d^{-1}$. Then, taking $H_{\rm hf}^{\rm d} = -0.21\times10^6$ Oe/$\mu_{\rm B}$ for ^{93}Nb [28] and the experimental $(T_1^{(e)}T)^{-1}$ value of 7.7 $s^{-1}K^{-1}$ at high temperatures, equation (3.2) with $C_{yz} + C_{zx} = 1$

gives $N(E_F) \sim 2.4$ 1 $eV^{-1}spin^{-1}$ which can reasonably be compared with 2.5 1 $eV^{-1}spin^{-1}$ obtained by the specific heat measurement [29]. The increase in $(T_1^{(e)}T)^{-1}$ observed below $\sim$50 K indicates a decrease in $N(E_F)$ by about 10% associated with the Peierls transition at T_{C1}.

The decrease in $N(E_F)$ below T_{C1} results in a decrease of negative K_d and, therefore, an increase of positive K_{iso} should be observed. The lack of the variation in the experimental K_{iso} below T_{C1} indicates that K_{iso} of ^{93}Nb in Nb_3Te_4 is dominated by the temperature-independent orbital term K_{VV}, in contrast to the dominant d spin contribution to $(T_1^{(e)}T)^{-1}$. The magnitude of K_d decrease is considered to be within the experimental uncertainty. The monotonic increase in ν_Q below $\sim$100 K (figure 4) is considered to mainly originate from the variation in q_{lat} associated with the superlattice formation.

A small amount of metal–atom intercalation into the hexagonal tunnels greatly modifies the physical properties of Nb_3Te_4 without intrinsic variations in the lattice constants and the energy band structure [13, 14]. The intercalation of 0.11 at.% In markedly enhances the electrical resistivity anomaly at T_{C1} and removes that at T_{C2}. In contrast, the intercalation of 0.1 at.% Zn completely removes the anomaly at T_{C1} and enhances the anomaly at T_{C2}. The increase in $T_1^{(e)}T$ observed below $\sim T_{C1}$ for $In_{0.11}Nb_3Te_4$ (figure 6) corresponds to a large extent of the Fermi surface quenching by about 44%, which is consistent with the enhanced resistivity anomaly at T_{C1}. For $Zn_{0.1}Nb_3Te_4$, on the other hand, $T_1^{(e)}T$ exhibits the nearly temperature-independent behaviour down to T_{C2} followed by the small increase, which corresponds to the partial Fermi surface quenching by about 16%. These results indicate a distinct nesting condition of the Fermi surface of $Zn_{0.1}Nb_3Te_4$ from that of $In_{0.11}Nb_3Te_4$.

The effect of the metal–atom intercalation appeared in the variations of relaxation rate, Knight shift and nuclear quadrupole frequency at high temperatures (table 1). The experimental increase in $(T_1^{(e)}T)^{-1}$ with the intercalation corresponds to the increase in DOS at E_F by 41% for 0.11 at.% In and by 35% for 0.1 at.% Zn. The large increase in $N(E_F)$, in spite of the small amount of intercalation, is consistent with the theoretical prediction that the Fermi level for Nb_3Te_4 is located near the minimum of the DOS curve.

The decrease in ν_Q with the intercalation gives, in a favourable case, a measure of hole doping. For the subbands of d_{yz}, d_{zx} and $d_{x^2-y^2}$ below E_F, equation (3.4) can be expressed as

$$q_{el} = \left(\frac{2}{7}n_{yz} + \frac{2}{7}n_{zx} - \frac{4}{7}n_{x^2-y^2}\right)\left\langle\frac{1}{r^3}\right\rangle. \tag{3.7}$$

For the present case of $n_{x^2-y^2} \gg n_{yz,zx}$, q_{el} takes a negative value and, therefore, gives a positive contribution of $(1+R)e^2q_{el}Q/24h$ ($Q < 0$) to the nuclear quadrupole frequency ν_Q. The hole doping initially reduces n_{yz} and/or n_{zx} of the dominant d subbands around E_F, and increases the positive $(1+R)e^2q_{el}Q/24h$. Then, the experimental decrease in ν_Q with the intercalation indicates that $(1-r_\infty)e^2q_{lat}Q/24h$ is negative and $|(1-r_\infty)q_{lat}| > |(1+R)q_{el}|$. The decrease in ν_Q by 0.4 MHz with 0.11 at.% In and 0.3 MHz with 0.1 at.% Zn intercalations suggests, at first sight, a comparable extent of hole doping between In and Zn. However, this cannot explain the distinct effect on the CDW formations of Zn intercalation from that of In intercalation.

It is worth noting that a remarkable difference between the In and Zn intercalation was observed only in the extent of K_{iso} decrease: $\simeq -0.02\%$ for 0.11 at.% In; $\simeq -0.07\%$ for 0.1 at.% Zn. This cannot simply be explained as an increase in the negative K_d caused by the increase in $N(E_F)$, because of almost the same amount of increase in $N(E_F)$ between the In and Zn intercalations. Then we have to take variations in K_{VV} and ν_Q simultaneously with the hole doping into consideration. The field-induced orbital susceptibility $\chi_{VV}^{\perp}$ perpendicular to the external field is given by

$$\chi^{\perp}_{\mathrm{VV}} = 2\mu_{\mathrm{B}}^2 \left\{ \frac{n_{yz}}{E(\mathrm{d}_{xy}) - E(\mathrm{d}_{yz})} + \frac{n_{zx}}{E(\mathrm{d}_{xy}) - E(\mathrm{d}_{zx})} \right\} + 2\mu_{\mathrm{B}}^2 \left\{ \frac{1}{E(\mathrm{d}_{yz}) - E(\mathrm{d}_{x^2-y^2})} + \frac{1}{E(\mathrm{d}_{zx}) - E(\mathrm{d}_{x^2-y^2})} \right\} n_{x^2-y^2}. \tag{3.8}$$

The hole doping initially reduces n_{yz} and/or n_{zx} and, following equations (3.1) and (3.8), decreases $K^{\perp}_{\mathrm{VV}}$, which is consistent with the experimental result for 0.11 at.% In intercalation.

On the other hand, the large decrease in K_{iso} with 0.1 at.% Zn intercalation could be explained if the extent of the hole doping with a Zn atom were much larger than that with an In atom. The heavy hole doping is able to greatly shift E_{F} to a lower energy level dominated by the $\mathrm{d}_{x^2-y^2}$ subband, through the bottom of the d_{yz} and/or d_{zx} subbands. For n_{yz} and/or $n_{zx} \to 0$, equation (3.8) gives a large decrease in $\chi^{\perp}_{\mathrm{VV}}$, whereas equation (3.7) gives an upturn of ν_{Q}. The change of the dominant subband at E_{F} from $\mathrm{d}_{yz,zx}$ for Nb_3Te_4 and $In_{0.11}Nb_3Te_4$ to $\mathrm{d}_{x^2-y^2}$ for $Zn_{0.1}Nb_3Te_4$ provides a distinct nesting condition of the Fermi surface.

4. Conclusion

The electronic state of a quasi-one-dimensional superconductor Nb_3Te_4 and their variations with a small amount of In and Zn intercalations into the hexagonal tunnels have been investigated microscopically with the ^{93}Nb NMR measurement. Below the Peierls transition temperature T_{C1} of Nb_3Te_4, the nuclear spin–lattice relaxation rate $(T_1T)^{-1}$ exhibits a decrease which corresponds to the partial Fermi surface quenching by about 12%. The nuclear quadrupole frequency ν_{Q} below T_{C1} exhibits a monotonic increase which is mainly caused by the superlattice formation associated with the Peierls transition.

With $x \simeq 0.1$ introductions of In and Zn, $(T_1T)^{-1}$ was greatly enhanced from 10 $\mathrm{s^{-1}K^{-1}}$ to 20 and 18 $\mathrm{s^{-1}K^{-1}}$, respectively. On the other hand, the nuclear quadrupole frequency ν_{Q} was diminished from 0.98 MHz to 0.63 and 0.74 MHz, respectively. A remarkable difference between the In and Zn intercalations was found in the extent of decrease in the isotropic Knight shift K_{iso}: from 0.237 to 0.216% for In, and to 0.166% for Zn.

Based upon the d band structures predicted theoretically, we have indicated that the variations in the NMR parameters can be explained consistently, if the extent of hole doping by a Zn atom is much larger than that by an In atom. The heavy hole doping by Zn intercalation changes the dominant subband at E_{F} from $\mathrm{d}_{yz,zx}$ to $\mathrm{d}_{x^2-y^2}$, giving rise to a distinct nesting condition of the Fermi surface for the Peierls transition.

References

[1] Selte K and Kjekshus A 1964 *Acta Crystallogr.* **17** 1568
[2] Ruysink A F, Kadijk F, Wagner A J and Jellinek F 1968 *Acta Crystallogr.* B **24** 1641
[3] Smeggil J G 1971 *J. Solid State Chem.* **3** 248
[4] Amberger E, Polborn K, Grimm P, Dietrich M and Obst B 1978 *Solid State Commun.* **26** 943
[5] Ishihara Y and Nakada I 1982 *Solid State Commun.* **42** 579
[6] Ishihara Y and Nakada I 1982 *Solid State Commun.* **44** 1439
[7] Oshiyama A 1983 *J. Phys. Soc. Japan* **52** 587
[8] Ishihara Y, Nakada I, Suzuki K and Ichihara M 1984 *Solid State Commun.* **50** 657
[9] Sekine T, Kikuchi Y, Matsuura E, Uchinokura K and Toshizaki R 1987 *Phys. Rev.* B **36** 3153
[10] Suzuki K, Ichihara M, Nakada I and Ishihara Y 1984 *Solid State Commun.* **52** 743
[11] Huan G and Greenblatt M 1987 *MRS Bull.* **22** 943
[12] Lee J-G, Chan S, Ramanujachary K V and Greenblatt M 1996 *J. Solid State Chem.* **121** 332
[13] Kagohashi T, Takarada T, Hasegawa H, Katumata Y, Kuga M, Okamoto H, Kaneko H and Ishihara Y 1999 *J. Phys.: Condens. Matter* **11** 6373

[14] Ohtani T, Yokota Y and Sawada H 1999 *Japan. J. Appl. Phys.* **38** L142
[15] Nakada I and Ishihara Y 1984 *J. Appl. Phys.* **23** 677
[16] Nakada I and Ishihara Y 1985 *J. Appl. Phys.* **24** 31
[17] Carter G C, Bennett L H and Kahan D J 1977 *Metallic Shifts in NMR* vol 1 (Oxford: Pergamon)
[18] Jones W H Jr, Graham T P and Barnes R G 1953 *Phys. Rev.* B **132A** 1898
[19] McCart B R 1965 *Thesis* Iowa State University, Ames, Iowa
[20] Narath A 1967 *Phys. Rev.* **162** 320
[21] Bullett D W 1980 *J. Solid State Chem.* **33** 13
[22] Oshiyama A 1982 *Solid State Commun.* **43** 607
[23] Oshiyama A 1983 *J. Phys. Soc. Japan* **52** 587
[24] Canadell E and Whangbo M H 1986 *Inorg. Chem.* **25** 1488
[25] Narath A 1967 *Hyperfine Interactions* ed A J Freeman and R B Frankel (New York: Academic) ch 7
[26] Cohen M H and Reif F 1957 *Solid State Physics* vol 5, ed F Seitz and D T Turnbull (New York: Academic)
[27] Obata Y 1963 *J. Phys. Soc. Japan* **18** 1020
[28] Yafet Y and Jaccarino V 1964 *Phys. Rev.* **133** A1630
[29] Okamoto H, Taniguti H and Ishihara Y 1996 *Phys. Rev.* B **53** 384